14

Integrated Vehicle Health Management for Solid Rocket Motors

D.G. Luchinsky[1,2], V.V. Osipov[1,2], V.N. Smelyanskiy[1], I. Kulikov[1], A. Patterson-Hein[1], B. Hayashida[3], M. Watson[3], D. Shook[4], M. Johnson[4], S. Hyde[4] and J. Shipley[4]

[1]*NASA Ames Research Center, MS 269-3, Moffett Field, CA, 94035,*
[2]*Mission Critical Technologies Inc., 2041 Rosecrans Ave., Suite 225 El Segundo, CA 90245,*
[3]*ISHM and Sensors Branch, NASA Marshall Space Flight Center, Huntsville, Alabama 35812,*
[4]*ATK Thiokol Launch Systems R&D Labs, Large Salt Lake City Area, Utah, USA*

1. Introduction

Solid rocket motors (SRMs) are an integral part of human space flight providing a reliable means of breaking away from the Earth's gravitational pull. The development and deployment of an integrated system health management (ISHM) approach for the SRMs is therefore a prerequisite for the safe exploration of space with the next-generation Crew and Heavy-Lift Launch Vehicles. This unique innovative technological effort is an essential part of the novel safety strategy adopted by NASA.

At the core of an on-board ISHM approach for SRMs are the real-time failure detection and prognostics (FD&P) technique. Several facts render the SRMs unique for the purposes of FD&P: (i) internal hydrodynamics of SRMs is highly nonlinear, (ii) there is a number of failure modes that may lead to abrupt changes of SRMs parameters, (iii) the number and type of sensors available on-board are severely limited for detection of many of the main SRM failure modes; (iv) recovery from many of the failure modes is impossible, with the only available resource being a limited thrust vector control authority (TVC); (iii) the safe time window between the detectable onset of a fault and a possible catastrophic failure is very short (typically a few seconds). The overarching goal of SRM FD&P is to extract an information from available data with precise timing and a highest reliability with no "misses" and no "false alarms". In order to achieve this goal in the face of sparse data and short event horizons, we are developing: (i) effective models of nominal and off-nominal SRM operation, learned from high-fidelity simulations and firing tests and (ii) a Bayesian sensor-fusion framework for estimating and tracking the state of a nonlinear stochastic dynamical system. We expect that the combination of these two capabilities will enable in-flight (real time) FD&P.

Source: Aerospace Technologies Advancements, Book edited by: Dr. Thawar T. Arif,
ISBN 978-953-7619-96-1, pp. 492, January 2010, INTECH, Croatia, downloaded from SCIYO.COM

Indeed, dynamical models of internal SRMs ballistics and many SRMs fault modes are well studied, see e.g. (Culick, 1996; Salita, 1989; Sorkin, 1967) and references therein. Examples of faults, for which quite accurate dynamical models can be introduced, include: (1) combustion instability; (ii) case breach fault, i.e. local burning-through of the rocket case; (iii) propellant cracking; (iv) overpressure and breakage of the case induced by nozzle blocking or bore choking. The combustion instabilities were studied in detail in the classical papers of (Culick & Yang, 1992; Culick, 1996) and (Flandro et al, 2004). Bore choking phenomenon due to radial deformation of the propellant grain near booster joint segments was studied numerically in (Dick et al., 2005; Isaac & Iverson, 2003; Wang et al., 2005) and observed in primary construction of the Titan IV (see the report, Wilson at al., 1992).
The FD&P system can be developed using the fact that many fault modes of the SRMs have unique dynamical features in the time-traces of gas pressure, accelerometer data, and dynamics of nozzle gimbal angle. Indeed, analysis shows that many fault modes leading to SRMs failures, including combustion instabilities (Culick,1974; Culick & Yang, 1992; Culick,1996; Flandro et al, 2004), bore choking (Dick et al., 2005; Isaac & Iverson, 2003; Wang et al., 2005), propellant cracking, nozzle blocking, and case breach (Rogers, 1986), have unique dynamical features in the time-traces of pressure and thrust. Ideally, the corresponding expert knowledge could be incorporated into on-board FD&P within a general Bayesian inferential framework allowing for faster and more reliable identification of the off-nominal regimes of SRMs operation in real time. In practice, however, the development of such an inferential framework is a highly nontrivial task since the internal ballistics of the SRMs results from interplay of a number of complex nonlinear dynamical phenomena in the propellant, insulator, and metal surfaces, and gas flow in the combustion chamber and the nozzle. On-board FD&P, on the other hand, can only incorporate low-dimensional models (LDMs) of the internal ballistics of SRMs. The derivation of the corresponding LDMs and their verification and validation using high-fidelity simulations and firing tests become an essential part of the development of the FD&P system.

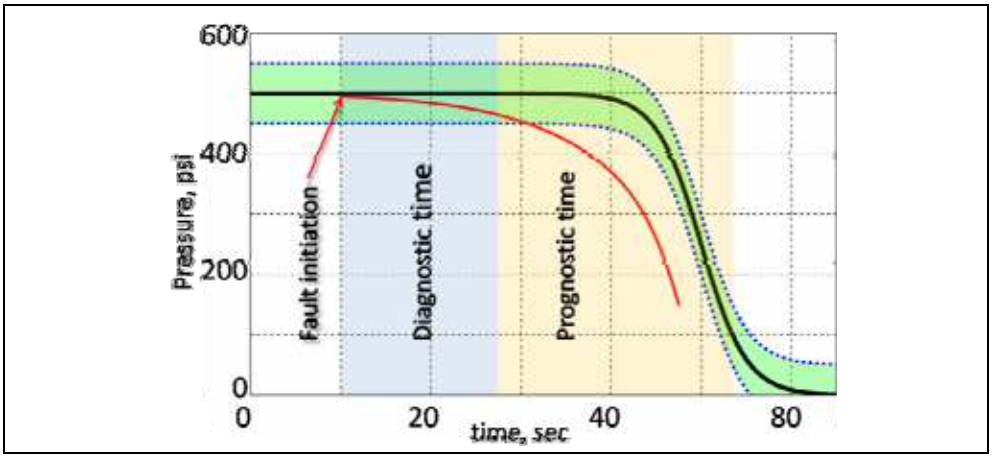

Fig. 1. Typical time-trace of pressure in the nominal regime is shown by the black line with pressure safety margins indicated by the green shading region. Fault-induced pressure time-trace in off-nominal regime is shown by the red line. Blue shading indicates diagnostic window and yellow shading indicates prognostic window.

At present the FD&P system in SRMs involves continuous monitoring of the time-traces of such variables as e.g. pressure, thrust, and altitude and setting up conservative margins on the deviation of these variables from their nominal values (see schematics in Fig. 1). However, in the absence of the on-board FD&P analysis of the SRM performance the probability of "misses" and "false alarms" is relatively high and reliability of the IVHM is reduced (see e.g. Rogers, 1986; Oberg, 2005). The goal of the on-board FD&P will be to detect the initiation time of the fault and provide its continuous diagnostic and prognostic while the performance variables are still within the safety margins to support the decision and to reduce the probability of "misses" and "false alarms".

In this chapter we report the progress in the development of such FD&P system. The main focus of our research was on the development of the: (i) model of internal ballistics of large segmented SRMs in the nominal regime and in the presence of number of fault modes including first of all case breach fault; (ii) model of the case breach fault; (iii) algorithms of the diagnostic and prognostic of the case breach fault within a general inferential Bayesian framework; and (iv) verification and validation of these models and algorithms using high-fidelity simulations and ground firing tests.

The chapter is organized as follows. In the next section we describe the low-dimensional performance model of internal ballistics of the SRMs in the presence of faults. In the Sec. III we modify this model for a subscale solid motor, analyze the axial distributions and validate the results of this model based on high-fidelity FLUENT simulations and analysis of the results of a ground firing test of the sub-scale motor faults. Developed Bayesian inferential framework for the internal SRM ballistics and FD&P algorithms is presented in the Sec. IV. FD&P for large segmented SRMs is analyzed in the Sec. V. Finally, in the Conclusions we review the results and discuss a possibility of extending proposed approach to an analysis of different faults.

2. Internal ballistics of the SRMs

The internal ballistics of the SRMs in the presence of the fault can be conveniently described by the following set of stochastic partial differential equations representing conservation laws for mass, momentum, and energy of the gas (Sorkin, 2005; Culick & Yang, 1992; Salita, 1989 & 2001)

$$\partial_t\left(UA_p\right)+\partial_x\left(f(U)A_p\right)=S, \tag{1}$$

where conservative variables of the gas dynamics and function $f(U)$ are given by the following equations

$$U=\begin{bmatrix}\rho\\ \rho u\\ \rho e_T\end{bmatrix},\quad f(U)=\begin{bmatrix}\rho u\\ \rho u^2+p\\ \rho u e_T+up\end{bmatrix}, \tag{2}$$

$e_T=c_VT+u^2/2$, $h_T=c_pT+u^2/2$, are the total energy and total enthalpy of the gas flow, $H=c_pT_0$ is the combustion heat of solid propellant and the source terms that include fault terms at a given location x_0 have the form

$$S=\begin{bmatrix} \rho_p \dot{R} l(x) - \rho_{t,h} u_{t,h} A_h \delta(x-x_0) + \xi_1(t) \\ p\partial_x A_p - \lambda \rho u^2 l(x) + \xi_2(t) \\ H\rho_p \dot{R} l(x) - h_{t,h} \rho_{t,h} u_{t,h} A_h \delta(x-x_0) + \xi_3(t) \end{bmatrix}. \quad (3)$$

This model extends the previous work (Salita, 1989 & 2001) in a number of important directions. To model various uncontrollable sources of noise (such as cracks and case vibrations) that may become essential in off-nominal conditions and may screen the variation of the system parameters a random component in the propellant density $\rho_p \rightarrow \rho_p[1+\sqrt{\sigma}\cdot\xi(t)]$ is introduced. Various faults can be modeled within the set of Eqs. (1)-(3) (including nozzle failure, propellant cracking, bore choking, and case breach) by choosing the time scale and direction of the geometrical alternations of the grain and case and the corresponding form of the sourse/sink terms. In particular, for the case breach fault two additional terms in the 1st and 3rd equations in Eqs. (3) correspond to the mass and energy flow from the combustion chamber through the hole in the rocket case with cross-section area $A_h(t)$. We now extend this mode by coupling the gas dynamics in the combustion chamber to the gas flow in the hole. The corresponding set of PDEs

$$\begin{cases} \partial_t (A_h \rho_h) = -\partial_x (A_h \rho_h u_h), \\ \partial_t (A_h \rho_h u_h) = -\partial_x (A_h \rho_h u_h^2) - A_h \partial_x p_h - f_{fr} l_h, \\ \partial_t (A_h \rho_h e_{t,h}) = -\partial_x [A_h \rho_h u_h h_{t,h}] - Q_h l_h, \end{cases} \quad (4)$$

resembles Eqs. (1). The important difference, however, is that we neglect mass flow from the walls of the hole. Instead Eqs. (4) include the term that describes the heat flow from the gas to the hole walls. The boundary conditions for this set of equations assume ambient conditions at the hole outlet and the continuity equation for the gas flow in the hole coupled to the sonic condition at the hole throat. The value of Q_h is presented in Eq. (14). The dynamics of the gas flow in the nozzle is described by a set of equations similar to (4) and can be obtained from this set by substituting subscript "n" for subscript "*h*".

The model (1)-(4) allow us to include possible burning rate variations and also various uncontrolled sources of noise, such as grain cracks and case vibrations to simulate more realistic time-series data representing off-nominal SRM operation. Due to the high temperature T of combustion products in the combustion chamber, the hot mixed gas can be considered as a combination of ideal gases. As we are interested in average gas characteristics (head pressure and temperature) we will characterize the combustion products by averaged parameters using the state equation for an ideal gas:

$$\frac{p}{\rho} = (c_P - c_V)T = \frac{p_0}{\rho_0}\left(\frac{T}{T_0}\right) = \frac{c_0^2}{\gamma}\left(\frac{T}{T_0}\right) \quad (5)$$

2.1 Regression of propellant surface

We take into account the propellant erosion in a large segmented rocket assuming that the erosive burning rate can be presented in the form

$$\dot{R} = r_b = ap^n + \dot{r}_{er}. \quad (6)$$

The erosive burning is taken into account in the Vilyunov's approximation

$$\dot{r}_{er} = C\left(I - I_{cr}\right) \tag{7}$$

for $I > I_{cr}$ and 0 otherwise, where C and I_{cr} are constants and I=const$(\rho u / r_b \rho_p)$Re$^{-1/8}$, where Re is the Reynolds number.

2.2 Model of the propellant geometry

To model the actual propellant geometry along the rocket axis the combustion chamber is divided into N segments as schematically shown in the Fig. 2. For each ballistic element the port area $A_p(x_i)$ and perimeter $l(x_i)$ averaged over the segment length dx_i are provided in the form of the design curves

$$A_p(x_i) = f_{Ai}(R(x_i)), \quad l(x_i) = f_{li}(R(x_i)) \tag{8}$$

(see Fig. 2). Note that the burning area and the port volume for each segment are given by the following relations

$$dV(x_i) = A_b(x_i)dx_i, \quad dA_b(x_i) = l(x_i)dx_i, \tag{9}$$

and, therefore, are uniquely determined by the burning rate r_{bi} for each ballistic element.
For numerical integration each segment was divided into a finite number of ballistic elements. The design curves were provided for each ballistic segment.

2.3 Model of the nozzle ablation

To model nozzle ablation we use Bartz' approximation (Bartz, 1965; Hill and Peterson,1992; Handbook, 1973) for the model of the nozzle ablation (Osipov et al., March 2007, and July 2007; Luchinsky et al., 2007) in the form:

$$\begin{aligned} \dot{R}_N &= v_{t0}\left(p / p_{\max}\right)^{1-\beta}\left(R_N / R_{t,in}\right)^{-\beta}\left[\left(T - T_{abl}\right)/\left(T_t - T_{abl}\right)\right], \\ v_{t0} &= \varepsilon C_p\left(\frac{\gamma p_{\max}}{\Gamma c_0}\right)^{1-\beta}\left(\frac{2R_{t,in}}{\mu}\right)^{-\beta}\frac{\left(T_t - T_{abl}\right)}{\left[c_{ins}\left(T_{abl} - T_0\right) + q_{ins}\right]}, \end{aligned} \tag{10}$$

where $\beta \approx 0.2$ and $\varepsilon \approx 0.023$. In a particular case of the ablation of the nozzle throat and nozzle exit this approximation is reduced to

$$\dot{R}_t = v_{m,t}\left(\frac{p_0}{p_{\max}}\right)^{1-\beta}\left(\frac{R_t}{R_{t,in}}\right)^{-\beta}, \quad A_t(t) = \pi R_t^2(t), \tag{11}$$

$$\dot{R}_{ex} = v_{m,ex}\left(\frac{p_0 A_t}{p_{\max} A_{ex}}\right)^{1-\beta}\left(\frac{R_{ex}}{R_{ex,in}}\right)^{-\beta}\frac{\left(T_{ex} - T_{abl}\right)}{\left(T_t - T_{abl}\right)}, \tag{12}$$

where $R_{t,in}$=$R_t(0)$, $R_{ex,in}$=$R_{ex}(0)$ and $v_{m,t}$ and $v_{m,ex}$ are experimentally determined constants. In practice, to fit experimental or numerical results on the nozzle ablation it suffice to put β = 0.2 and to obtain values of $v_{m,t}$ and $v_{m,ex}$ by regression.

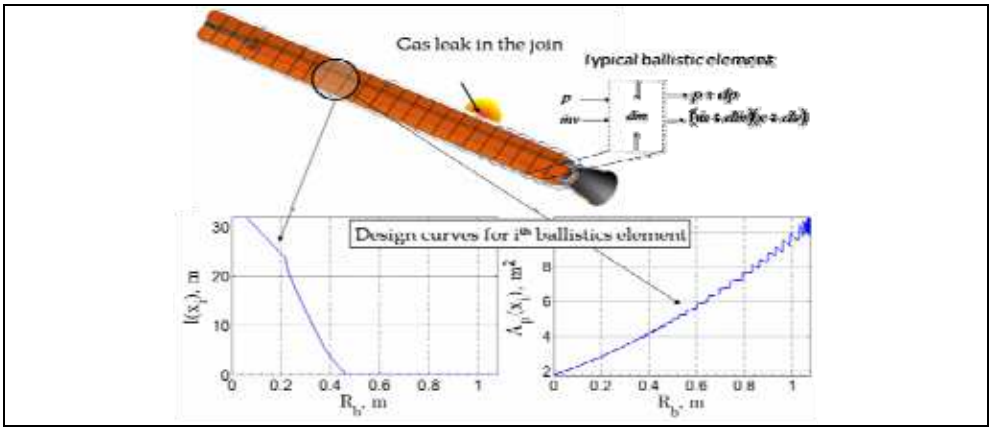

Fig. 2. Sketch of a cross-section of an idealized geometry of the multi-segment RSRMV rocket and an example of the design curves (8) for the head section.

2.4 Model of the burning-though of a hole

To complete the model of the case breach fault for the segmented SRMs the system of equations (1)—(12) above has to be extended by including equations of the hole growth model (Osipov et al., 2007, March and 2007, July; Luchinsky et al., 2007)

$$\dot{R}_h = v_h(p_{t,h}, T_{h,t}) = \frac{Q_c + Q_R + Q_b}{\left[q_{met} + C_{met}\left(T_{mel} - T_{m0}\right)\right]\rho_{met}}, \tag{13}$$

$$\begin{aligned} Q_R &= \sigma\left[1 - \exp\left(-\lambda p_{t,h}\right)\right]\left(T_t^4 - T_{met}^4\right), \\ Q_c &= 0.023 C_p \left(\frac{\gamma p_{t,h}}{\Gamma c_0}\right)^{0.8} \left(\frac{2R_h}{\mu}\right)^{-0.2} \left(T_t - T_{met}\right), \\ Q_b &= v_{fb}\left[q_{met} + C_{met}\left(T_{mel} - T_{m0}\right)\right]\rho_{met}. \end{aligned} \tag{14}$$

Here $Q_h = Q_c + Q_R + Q_b$.

3. A subscale motor

Motivated by the results of the ground firing test let us consider an application of the model (1)-(14) to an analysis of the case breach fault in a subscale motor. Note that a subscale motor can be consider as model (1)-(14) consisting of one ballistic element. In this case the velocity of the flow is small and one can neglect the effects of erosive burning, surface friction, and the variation of the port area along the motor axis.

3.1 SRM internal ballistics in the "filling volume" approximation

To derive the LDM of the case breach fault we integrate equations (1) along the rocket axis and obtain the following set of ordinary differential equations for the stagnation values of the gas parameters and the thickness of the burned propellant layer

$$\begin{cases} \partial_t\left(\rho_0 V\right) = -\left(\rho u A\right)\big|_L + \rho_p r_b(p_0) A_b + A_1\xi_1(t), \\ \partial_t\left(\rho_0 e_0 V\right) = -\left(\rho u A h_t\right)\big|_L + H\rho_p r_b(p_0) A_b + A_2\xi_2(t), \\ \partial_t R = r_b\left(p_0\right). \end{cases} \tag{15}$$

Here $(\rho uA)\,|_L$ and $(\rho uAh_t)\,|_L$ are the mass and the enthalpy flow from the whole burning area of the propellant including the propellant surface in the hole and p_0, ρ_0, and e_0 are the stagnation values of the flow parameters. The total mass flow from the burning propellant surface is equal to the sum of the mass flows through the nozzle' and hole throats. Assuming that sonic conditions hold both in the nozzle throat and the hole throat we obtain the following result

$$\begin{aligned} \left(\rho uA\right)\big|_L = \left(\rho_h u_h A_h\right)\big|_t + \left(\rho uA\right)\big|_t = \\ \Gamma^{-1}\sqrt{\gamma\rho_0 p_0}\,A_{t,h} + \Gamma^{-1}\sqrt{\gamma\rho_0 p_0}\,A_t = \Gamma^{-1}\sqrt{\gamma\rho_0 p_0}\left(A_{t,h} + A_t\right) \end{aligned} \tag{16}$$

Here $\Gamma=((\gamma+1)/2)^{(\gamma+1)/2(\gamma-1)}$ and $A_{et}=(A_{t,h}+A_t)$ is the effective nozzle throat area. This relation means that in the first approximation the hole is seen by the internal flow dynamics as an increase of the nozzle throat area and the dynamics of the stagnation values of the gas parameters are governed by both dynamics of the propellant burning area (related to the thickness of the burned propellant layer R) and by the hole radius R_h. Substituting results of integration (16) into (15) and using model for nozzle ablation (11), (12) and hole melting (13), (14) we obtain the low-dimensional model of the internal ballistic of a subscale SRM in the presence of the case breach fault in the form

$$\begin{aligned} &\dot\rho = -\frac{c_0\Gamma A_{et}}{V r_b}\rho\sqrt{\frac{p}{\rho}} + \frac{A_b}{V}\left(\rho_p - \rho\right)p^n + a_1\xi_1(t), \\ &\dot p = -\frac{c_0\gamma\Gamma A_{et}}{V r_b}p\sqrt{\frac{p}{\rho}} + \frac{A_b}{V}\left(\gamma\rho_p - p\right)p^n + a_2\xi_2(t), \\ &\dot R = r_b p^n, \quad A_b = f(R), \quad \dot V = A_b\dot R = f(R) r_b p^n, \\ &\dot R_t = v_{abl} = v_m\left(\frac{p_0}{p_m}\right)^{1-\beta}\left(\frac{R_t}{R_{t0}}\right)^{-\beta}, \\ &\dot R_{ex} = v_m\left(\frac{p_0 A_t}{p_m A_{ex}}\right)^{1-\beta}\left(\frac{R_{ex}}{R_{ex0}}\right)^{-\beta}\frac{\left(T_{ex} - T_{abl}\right)}{\left(T_t - T_{abl}\right)}, \\ &\dot R_h = \frac{Q_c + Q_R + Q_b}{\left[q_{met} + C_{met}\left(T_{mel} - T_{m0}\right)\right]\rho_{met}}, \end{aligned} \tag{17}$$

where the following dimensionless variables are used

$$p \to \frac{p_0}{p_m},\ \rho \to \frac{\rho_0}{\rho_m},\ t \to \frac{t r_b(p_m)}{L_0},\ R_t \to \frac{R_t}{L_0},\ A_b \to \frac{A_b}{L_0^2},\ V \to \frac{V}{L_0^3},\ R_{t,h} \to \frac{R_{t,h}}{L_0},\ R \to \frac{R}{L_0},\ A_{et} \to \frac{A_{et}}{L_0^2}. \tag{18}$$

Here subscript m refers to maximum reference values of the pressure and density and L_0 is characteristic length of the motor. We note that two first equations in (17) correspond to the "filling volume" approximation in (Salita, 1989 & 2001). The important difference is that we have introduced noise terms and the exact dependence of the burning surface on the burn distance in the form of the design curve relation in the fourth equation in (17). We have also established an explicit connection with the set of partial differential equations (1) that helps to keep in order various approximations of the Eqs. (1), which are frequently used in practice and in our research.
The equations above have to be completed by the equations for the main thrust F and lateral (side) thrust F_h induced by the gas flow through the hole in the form

$$F = \Gamma^{-1}\sqrt{\gamma\rho_0 p_0}\,A_t u_{ex} + (p_{ex} - p_a)A_{ex}, \quad F_h = \Gamma^{-1}\sqrt{\gamma\rho_0 p_0}\,A_{t,h}u_{h,ex} + (p_{ex,h} - p_a)A_{h,ex} \qquad (19)$$

where p_a is ambient pressure, u_{ex} and $u_{h,ex}$ are gas velocities at the nozzle outlet and hole outlets respectively, and p_{ex} and $p_{h,ex}$ are the exit pressure at the nozzle outlet and hole outlets respectively.

3.2 Axial distributions of the flow variables in a sub-scale motor

It follows from the analysis that $M_0^2 = v^2/c_0^2 \ll 1$ is small everywhere in the combustion chamber. Furthermore, the equilibration of the gas flow variables in the chamber occurs on the time scale ($t = L/c$) of the order of milliseconds. As a result, the distribution of the flow parameters follows adiabatically the changes in the rocket geometry induced by the burning of the propellant surface, nozzle ablation and metal melting in the hole through the case. Under these conditions it becomes possible to find stationary solutions of the Eqs. (1) analytically in the combustion chamber. Taking into account boundary conditions at the stagnation point and assuming that the spatial variation of the port area $A_p(x)$ is small and can be neglected together with axial component of the flow at the propellant surface $u_S(x)$, we obtain the following equations for the spatial variation of the flow parameters (Osipov et al., March 2007)

$$\left(S\rho u\right)\Big|_0^x = \int_0^x \rho_p r_b l dx, \quad \rho u^2 + p = p_0, \quad \left(S\rho h_t u\right)\Big|_0^x = H\int_0^x \rho_p r_b l dx. \qquad (20)$$

$$\rho = \rho_0\left(1+\frac{\gamma+1}{2}\frac{u^2}{c_0^2}\right)^{-1}, \; p = p_0\left(1+\frac{\gamma+1}{2}\frac{u^2}{c_0^2}\right)^{-1}\left(1-\frac{\gamma-1}{2}\frac{u^2}{c_0^2}\right)^{-1}, \; v = \frac{u_L x}{L}\left(1+\frac{3(\gamma+1)-2n\gamma)}{6c_0^2}u_L^2\frac{x^2}{L^2}\right). \qquad (21)$$

and in the nozzle area

$$p = p_0\left(1-\frac{(\gamma-1)}{2}M_0^2\right)^{\frac{\gamma}{\gamma-1}}, \quad \rho = \rho_0\left(1-\frac{(\gamma-1)}{2}M_0^2\right)^{\frac{1}{\gamma-1}}, \quad T = T_0\left(1-\frac{(\gamma-1)}{2}M_0^2\right), \qquad (22)$$

where M_0 is given by the solution of the nozzle equation

$$M_0\left(1-\frac{(\gamma-1)}{2}M_0^2\right)^{\frac{1}{\gamma-1}} = \frac{A_t}{\Gamma A}.$$

3.3 Verification and validation (V&V) of the "filing volume" model

To verify the model we have performed high-fidelity simulations using code by C. Kiris (Smelyanskiy et al., 2006) and FLUENT model (Osipov et al., 2007; Luchinsky et al., 2008). To solve the above system of equations numerically we employ a dual time-stepping scheme with second order backward differences in physical time and implicit Euler in psuedo-time, standard upwind biased finite differences with flux limiters for the spatial derivative and the source terms are evaluated point-wise implicit. For these simulations the following geometrical parameters were used: initial radius of the grain R_0 = 0.74 m, R_t = 0.63 m, L = 41.25m; ρ = 1800 kg·m^{-3}, H = 2.9x106 J·kg^{-1}, r_c = 0.01 m·sec^{-1}, p_c = 7.0x10^6 Pa. The results of integration for a particular case of the neutral thrust curve are shown in the Fig. 1(b). The fault (the nozzle throat radius is reduced by 20%) occurs at time t_f = 15 sec. The comparison of the results of the simulations of the model (1) with the solution of the LDM (17) is shown in the Fig. 3(a). It can be seen from the figure that the LDM reproduces quite accurately the dynamics of the internal density in the nominal and off-nominal regimes. Similar agreement was obtained for the dynamics of the head pressure and temperature.

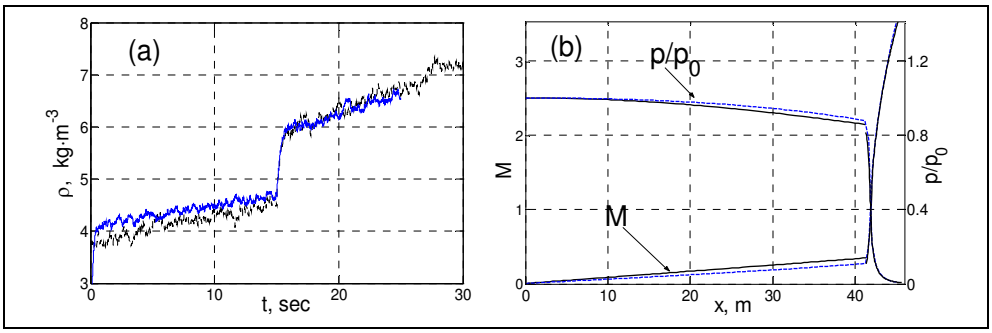

Fig. 3. (a) Comparison between the results of integration of the stochastic partial differential equations Eqs. (1), (2)(solid blue lines) and stochastic ordinary differential equations Eqs. (17)(dotted black lines) for the time evolution of the head density. (b) Comparison between the numerical (dashed blue lines) and analytical (solid lines) solutions for the gas velocity and pressure.

The comparison of the analytical solution (21), (22) for axial distribution of the pressure and velocity with the results of numerical simulation of the high-fidelity model is shown in the Fig. 3(b). It can be seen from the figure that the axial variation of the gas flow parameters is small and agrees well with the results of numerical integration. Therefore, the dynamics of the SRMs operation with small variation of the port area along the rocket axis can be well characterized by the LDM (17), obtained by integration of Eqs. (1), (2) over the length of the combustion camera.

This conclusion is also supported by the 2D high-fidelity simulations using FLUENT. To simulate time evolution of the propellant regression, nozzle ablation, and the hole burning through we have introduced the following deforming zones (see Fig. 4): (i) hole in the forward closure; (ii) nozzle ablation; and (iii) variation of the burning area as a function of time. In simulations we have used a density based, unsteady, implicit solver. The mesh was initialized to the stagnation values of the pressure, temperature, and velocity in the combustion chamber and to the ambient values of these variables in the two ambient

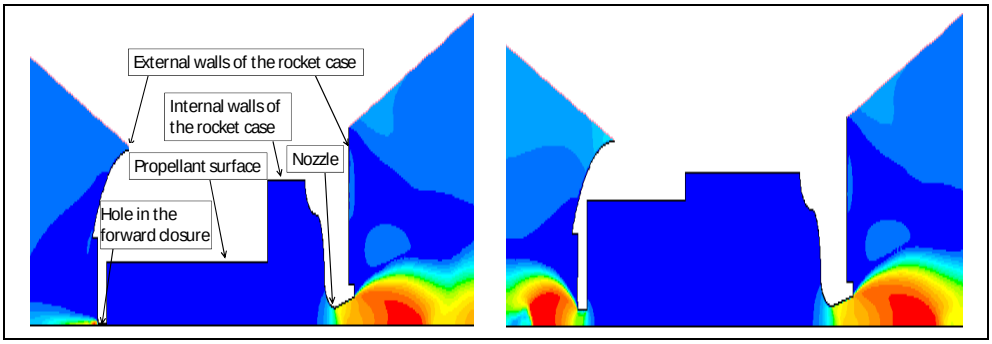

Fig. 4. 2D velocity distribution with axial symmetry obtained using FLUENT simulations after 0.14 sec (left) and t = 5.64 (right). The geometry of the model surfaces is shown in the figure. The propellant surface wall, hole wall, and the nozzle wall are deforming according to the equations (2), note the changes in the geometry of the rocket walls and the corresponding changes in the velocity distribution.

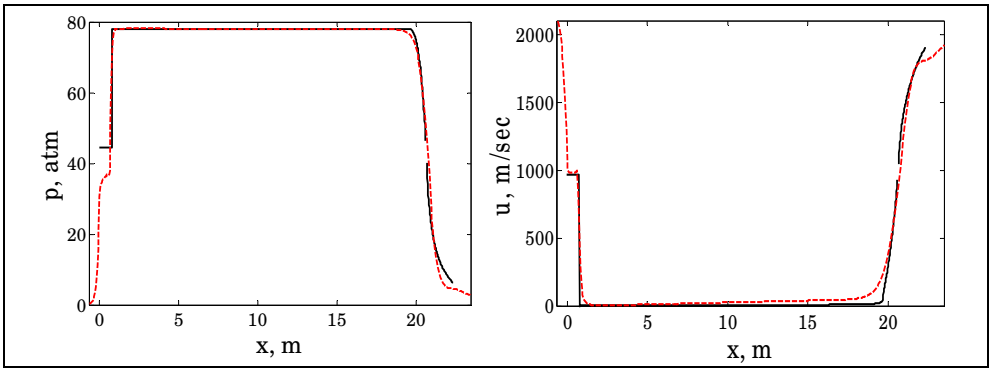

Fig. 5. Axial velocity (left) and pressure (right) profiles generated by the FLUENT model for t=0.05 sec (red dashed line) as compared to the analytical solutions (black solid lines) given by the (21), (22).

regions on the right and left of the chamber. The results of the comparison of the analytical distributions (21)-(22) with the axial velocity and pressure distributions obtained using FLUENT simulations are shown in the Fig. 5. It can be seen from the figure that the model (17), (21)-(22) provides a very good approximation to the results of FLUENT simulations.
Note that the difference in the time scales for dynamics of burn distance, metal erosion, and nozzle ablation as compared to the characteristic relaxation time of the distributions to their quasi-stationary values t_{rel} allows us to integrate equations (1), (2) in quasi-stationary approximation as will be explained in details in Sec. 5. As a result we obtain the analytical solution for the quasi-stationary dynamics of the axial distributions of the gas parameters in the combustion chamber and in the nozzle area. The comparison of this analytical solution with the results of FLUENT simulations also demonstrates agreement between the theory and numerical solution of the high-fidelity model. The accuracy of the low-dimensional model (17) was further validated using results of a ground firing test for a subscale motor as will be described in details elsewhere.

4. Bayesian inferential framework for internal SRMs ballistics

We are now in a position to introduce a novel Bayesian inferential framework for the fault detection and prognostics in SRMs. Note that the effect of the case breach fault and nozzle blocking on the dynamics of the internal gas flow in SRMs is reduced to the effective modification of the nozzle throat area $A_{et}(t)$ as explained above. In a similar manner the effects of bore choking and propellant crack can be taken into account by introducing an effective burning area and by coupling the analysis of the pressure time-traces with the analysis of the nozzle and side thrust. The accuracy of the calculations of the internal SRM ballistics in sub-scale motors in nominal and off-nominal regimes based on the LDM (17) allows us to use it to verify the FD&P in numerical simulations.

4.1 Bayesian framework

The mathematical details of the general Bayesian framework are given in (Luchinsky et al., 2005). Here we briefly introduce earlier results in the context of fault detection in SRMs including abrupt changes of the model parameters. The dynamics of the LDM (17) can be in general presented as an Euler approximation of the set of ODEs on a discrete time lattice $\{t_k=hk; k=0,1,...,K\}$ with time constant h

$$x_{k+1} = x_k + hf(x_k^* \mid c) + \hat{\sigma}\sqrt{h}z_k, \tag{23}$$

where $z_k = \frac{1}{\sqrt{h}}\int_{t_k}^{t_k+h} \xi(t)dt$, $x_k^* = \frac{x_k + x_{k+1}}{2}$, $\boldsymbol{x_k} = \{p, \rho, R, V, r_h, r_t, r_i\}$ is L-dimensional state of the system (17), σ is a diagonal noise matrix with two first non-zero elements a_1 and a_2, $\boldsymbol{f}$ is a vector field representing the rhs of this system, and c are parameters of the model. Given a Gaussian prior distribution for the unknown model parameters, we can apply our theory of Bayesian inference of dynamical systems (Luchinsky et al., 2005) to obtain

$$D_{ij} = \frac{h}{K}\sum_{k=0}^{K-1} (\dot{x}_k - f(x_k;c))_i (\dot{x}_k - f(x_k;c))_j \tag{24}$$

$$c'_l = (A)^{-1}_{ml} w_m, \tag{25}$$

where elements A_{ml} and w_m are defined by the following equations

$$w_m = h\sum_{k=0}^{K-1}\left[\sum_{n,n'=1}^{L} U'_{mn}(t_k) D^{-1}_{nn'} \dot{x}_{n'}(t_k) - \frac{v_m}{2}\right] \tag{26}$$

$$A_{ml} = h\sum_{k=0}^{K-1}\left[\sum_{n,n'=1}^{L} U'_{mn}(t_k) D^{-1}_{nn'} U_{n'l}(t_k)\right]. \tag{27}$$

Here the vector field is parameterized in the form $f(x;c)=\hat{U}(x)c$, where $\hat{U}(x)$ is a block-matrix with elements U_{mn} build of N blocks of the form $\hat{I}\phi_n(x(t_k))$, $\hat{I}$ is LxL unit matrix, and

$$\mathrm{v}_m(\mathbf{x}) = \sum_{n=1}^{N} \frac{\partial U_{nm}(\mathbf{x})}{\partial x_n}.$$

To verify the performance of this algorithm for the diagnostics of the case breach fault we first assume the nominal regime of the SRM operation and check the accuracy and the time resolution with which parameters of the internal ballistics can be learned from the pressure signal only. To do so we notice that equations for the nozzle throat radius r_t, burn distance R, and combustion chamber volume can be integrated analytically for a measured time-traces of pressure and substituted into the equations for pressure dynamics. By noticing further that for small noise-intensities the ratio of dimensionless pressure and density $p/\rho \approx 1$ obtain the following equation for the pressure dynamics

$$\dot{p} = -\frac{c_0 \gamma \Gamma A_{et}}{V r_b} p + \frac{A_b}{V}\left(\gamma \rho_p - p\right) p^n + \sqrt{D}\xi_2(t), \tag{28}$$

where $A_t(t)$, $A_b(t)$, and $V(t)$ are known functions of time given by the following equations

$$\begin{aligned} &R(t) = \int_0^t p^n(t')dt', \quad A_b(t) = f\left(R(t)\right), \quad V(t) = V_0 + \int_0^{R(t)} A_b(R)dR, \\ &A_t(t) = \pi r_t^2(t), \quad R_t(t) = \left[R_{t0}^{1+\beta} + v_m(1+\beta)\int_0^t p^{1-\beta}(t')dt' \right]^{\frac{1}{1+\beta}} \end{aligned} \tag{29}$$

The parameters $c_0\gamma\Gamma/r_b$, $\gamma\rho_p$, and D can now be inferred in the nominal regime by applying Eqs. (23)-(27) to the analysis of equation (28). An example of the inference results is shown in the Table 1.

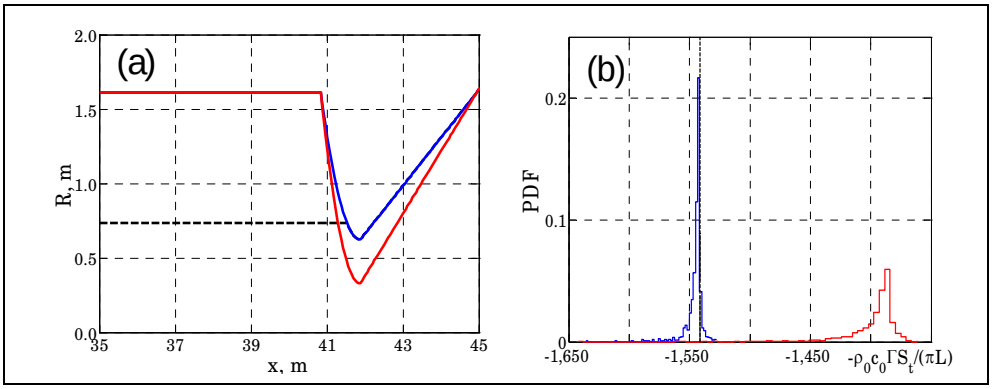

Fig. 6. (a) An example of the geometry of the simulations of the nozzle failure model using Eqs. (1), (2). The geometry of the case before and after the fault is shown by the solid blue and red lines respectively. (b) estimation of the value of the parameter $-c_0GA_t/(pL)$ before (left curve) and after (right curve) the fault. The dashed line shows the actual value of the parameter. The solid lines show the PDF of the parameter estimation with T=0.1 sec, Δt=0.001 sec, N=500 (see the caption for the Table 1).

Parameters	Actual	Inferred	Relative error
$\gamma\rho_p$	248.2	244.7	1.4%
$-c_0\Gamma/r_b$	-61260	-61347	1.38%
D	2.5×10^{-4}	2.44×10^{-4}	2.4%

Table 1. The results of the parameter estimation of the model (28), (29) in the nominal regime. The total time of the measurements in this test was T=1 sec, the sampling rate was 1 kHz, and the number of measured points was N=1000.

We conclude that the parameters of the nominal regime can be learned with good accuracy during the first few second of the flight. This result allows one to apply Bayesian algorithm for fault detection and diagnostics in SRMs.

We now provide numerical example explaining in more details how this technique can be used for in-flight FD&P in SRMs. We will be interested to verify if the Bayesian framework can provide additional information ahead of the "alarm" time about the most likely course of the pressure dynamics to reduce the probability of the "misses" and "false alarms". To model the "miss" situation a case will be considered when small pressure deviation from the nominal value persists for a few second prior to the crossing the "alarm" level and the time window between the "alarm" and "catastrophe" becomes too short. This situation is illustrated in the Fig. 7(a), where measured pressure signal (black solid line) crosses the alarm level (dashed line) initiating the alarm at approximately $t_A \approx 15$ sec. The overpressure fault occurs at $t_F \approx 17$ sec and the time window between the alarm and a "catastrophic" event becomes too short, which can be considered as a model of "miss" situation. To model the "false alarm" situation a case will be considered in which the pressure crosses the "alarm" level, but then returns to its nominal value (see Fig. 7(b)). In all the simulations presented here the overpressure fault was modeled as a reduction of the nozzle throat area. Note, however, that the results discussed below can be extended to encompass other faults, including e.g. the propellant cracking, bore choking, and case breach as will be discussed below.

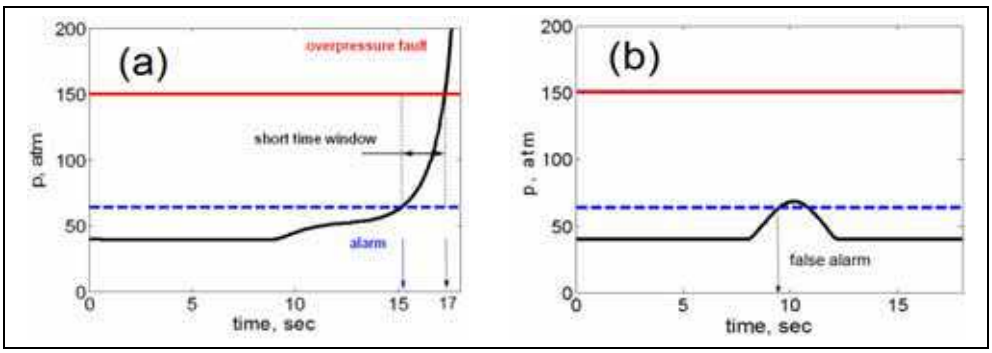

Fig. 7. (a) Example of possible time variation of the pressure fault (black line) representing a possible "miss" situation. The blue dashed and red solid lines indicate the "alarm" and the "catastrophe" levels respectively. Note that the time window between the "alarm" and the "catastrophe" is too short. (b) Example of possible time variations of the fault pressure representing a possible "false alarm" situation. The blue dashed and red solid lines are the same as in (a).

4.2 Modeling "misses" for the nozzle failure and neutral thrust curve

To model the "misses" we assume that the time evolution of the nozzle fault is highly nonlinear and can be described by a polynomial function

$$A_{et} = A_{t0} - \Delta A\left(\alpha\tau + \beta\tau^2 + \delta\tau^3\right) \tag{30}$$

corresponding e.g. to the slow degradation followed by the fast destruction of the nozzle walls as shown in the Fig. 7(a), where τ is the time elapsed from the fault initialization. In this case the time window between the "alarm" and the overpressure fault becomes too short and effectively the FD&P system "misses" the event. The thrust curve is chosen to be neutral. Our goal is to demonstrate that application of the Bayesian framework for the SRM FD&P allows one to extend substantially the time window between the "alarm" and the overpressure fault thereby reducing the probability of "misses". To this end we extend the model described by Eqs. (17) by including nonlinear terms from Eq.(30). The corresponding vector field of the Eq. (28) can be written as $f(x;c)=\hat{C}\phi$ with the set of the base functions given by Eq. (31) and the set of the model parameters is given in Eq.(32), where $a=(c_0\Gamma)/(\pi L r_{b0} R^*)$.

$$\vec{\phi} = \left\{ p^n, \frac{p^n}{R}, \frac{p^{n+1}}{R}, \frac{p^n\rho}{R}, \sqrt{\frac{p}{\rho}}\frac{p}{R}, \sqrt{\frac{p}{\rho}}\frac{p\tau}{R}, \sqrt{\frac{p}{\rho}}\frac{p\tau^2}{R}, \sqrt{\frac{p}{\rho}}\frac{p\tau^3}{R}, \ldots \right.$$
$$\left. \sqrt{\frac{p}{\rho}}\frac{\rho}{R}, \sqrt{\frac{p}{\rho}}\frac{\rho\tau}{R}, \sqrt{\frac{p}{\rho}}\frac{\rho\tau^2}{R}, \sqrt{\frac{p}{\rho}}\frac{\rho\tau^3}{R} \right\} \tag{31}$$

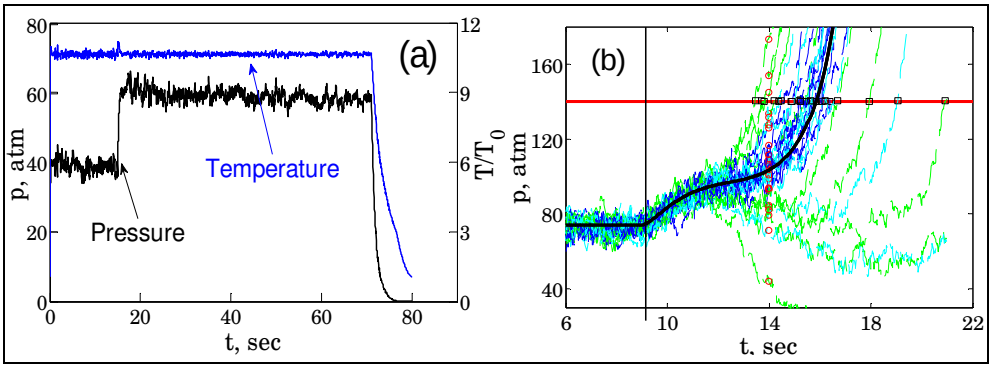

Fig. 8.(a) An example of the time-traces of temperature (blue line) and the pressure (black line) of the SRM operation with neutral thrust curve. Fault corresponding to abrupt changes of the nozzle throat area (cf Fig. 6(a)) occurs at t=17 sec. (b) Nonlinear time evolution of the pressure build up after the nozzle blocking fault is shown by the back solid line. Predicted dynamics of the pressure is shown by the jiggling lines. The results of the predictions build 1sec, 1.5sec, and 2.1 sec after the fault are shown by green, cyan, and blue lines correspondingly. The values of the pressure at t=14 sec, which are used to build the PDF of the pressure, are shown by red circles. The time moments of the predicted overpressure faults used to build the PDF of the case burst times as shown by the black squares on the red margin line. Fault occurs at t=9 sec.

$$\hat{C} = \begin{bmatrix} 0 & 2\gamma\rho_p & -2 & 0 & -a\gamma & -a\gamma\alpha & -a\gamma\beta & -a\gamma\delta & 0 & 0 & 0 & 0 \\ 0 & 2\rho_p & 0 & -2 & 0 & 0 & 0 & 0 & -a & -a\alpha & -a\beta & -a\delta \\ 1 & 0 & 0 & 0 & 0 & 0 & 0 & 0 & 0 & 0 & 0 & 0 \end{bmatrix} \quad (32)$$

Parameters of the system are monitored in real time. Once small deviations from the nominal values of the parameters is detected at time t_d the algorithm is continuously updating the inferred values of parameters estimated on increasing intervals Δt of time elapsed from t_d . These values are used to generate a set of trajectories predicting pressure dynamics. Example of such sets of trajectories calculated for three different time intervals Δt =1sec, 1.5 sec, and 2.1 sec are shown in the Fig. 8(b) by green, cyan, and blue lines respectively. These trajectories are used to predict the PDFs of the head pressure for any instant ahead of time. An example of such PDF for the pressure distribution at time at t=14 sec is shown in the Fig. 9(a). The method used to calculate PDF for the pressure distributions is illustrated in the Fig. 8(b). The same trajectories are used to predict the PDFs of the time moment of the overpressure fault as illustrated in the Fig. 8(b) and Fig. 9(b). It can be seen from the figures that the distribution of the predicted time of the overpressure fault converges to the correct value 2.1 sec after the fault thereby extending the time window between the "alarm" and the fault to 6 sec which is almost three folds of the time window obtained using standard technique.

Therefore, we conclude that the Bayesian framework provides valuable information about the system dynamics and can be used to reduce the probability of the "misses" in the SRM FD&P system. A similar analysis shows (Luchinsky et al., 2007) that the general Bayesian framework introduced above can be applied to reduce the number of "false alarms".

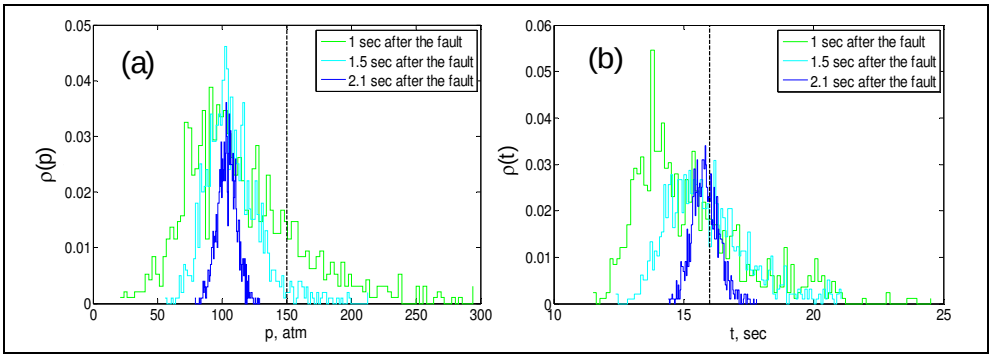

Fig. 9. (a) The PDF of the predicted values of pressure at t=14 sec build 1 sec (green line), 1.5 sec (cyan line), and 2.1 sec (blue lines) after the fault. The dashed vertical line shows the dangerous level of the pressure. (b) The PDF of the predicted times of the overpressure fault build 1sec (green line), 1.5 sec (cyan line), and 2.1 sec (blue lines) after the fault. The dashed vertical line shows the actual time when the overpressure fault is going to happen.

4.3 Self-consistent iterative algorithm of the case breach prognostics

In the previous section we have shown that in-flight FD&P for SRMs can be developed within Bayesian inferential framework. The introduced technique can be very useful in a wide range of contexts including in particular active control of combustion instabilities in

liquid motors (Hathout et al, 2002). In practice, however, it is often desirable (see also the following section) to further simplify the algorithm by avoiding stochastic integration. The simplification can be achieved by neglecting noise in the pressure time-traces and by considering fault dynamics in a regime of quasi-steady burning.

To illustrate the procedure of building up iterative FD&P algorithms that avoids stochastic integration let us consider the following example problem. A hole through the metal case and insulator occurs suddenly at the initial time of the fault t_0. The goal is to infer and predict the dynamics of the growth of the holes in the insulator layer and in the metal case, as well as the fault-induced side thrust, and changes to the SRM thrust in the off-nominal regime. In this example the model for the fault dynamics is assumed to be known. This is a reasonable assumption for the case breach faults with simple geometries. For this case the equations can be integrated analytically in quasi-steady regime and the prognostics algorithm can be implemented in the most efficient way using a self-consistent iterative procedure, which is developed below. As an input, we use time-traces of the stagnation pressure in the nominal regime and nominal values of the SRM parameters. In particular, it is assumed that the ablation parameters for the nozzle and insulator materials and the melting parameters for the metal case are known. It is further assumed that the hole radius in the metal case is always larger than the hole radius in the insulator (i.e. the velocity of the ablation of the insulator material is smaller than the velocity of the melting front), accordingly the fault dynamics is determined by the ablation of the insulator. This situation can be used to model damage in the metal case induced by an external object.

To solve this problem we introduce a prognostics algorithm of the fault dynamics based on a self-consistent iterative algorithm that avoids numerical solution of the LDM. We notice that with the limit of steady burning, the equations in (17) can be integrated analytically. Because the hole throat is determined by the radius of the hole in the insulator, we can omit the equation for the hole radius in the metal case. The resulting set of equations has the form

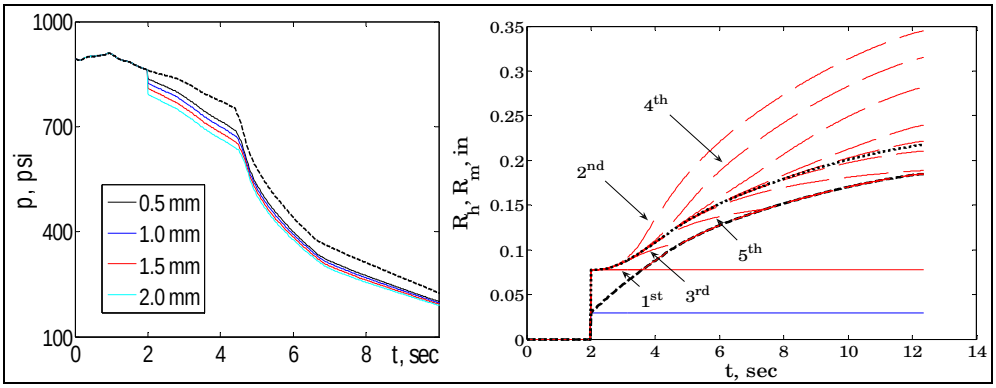

Fig. 10. (left) Results of the calculations using iterative algorithm A1. Absolute values of pressure for four different initial values of the hole in the case: 0.5, 1.0, 1.5 and 2.0 mm are shown by the black, blue, red, and cyan solid lines respectively. The nominal pressure is shown by the dashed black line. (right) Iterations of the effective hole radius in the metal case. Red solid line shows 0th approximation. Five first approximations shown by red dashed lines are indicated by arrows. Final radius of the hole in the metal case is shown by black dotted line. 0th approximation for the hole in the insulator is shown by dashed blue line. Final radius of the hole in the insulator is shown by the black dashed line.

$$\begin{cases} p(t) = p_N(t)\left[\dfrac{A_{bef}(t)A_t(t)}{A_b A_{et}(t)}\right]^{\frac{1}{1-n}}, \\ R = a\int\limits_0^t p^n(\tau)d\tau, \\ R_t^{1+\beta_t}(t) = R_{t0}^{1+\beta} + (1+\beta)v_{n0}\int\limits_{t_0}^t p^{1-\beta}(\tau)d\tau, \\ R_h^{1+\beta_i}(t) = R_{h0}^{1+\beta_i} + (1+\beta)v_{h0}\int\limits_{t_0}^t p^{1-\beta}(\tau)d\tau. \end{cases} \quad (33)$$

Here $A_{et}(t) = A_t(t) + \Delta A_t(t) + A_h(t)$ is an effective nozzle throat area where the 1st term corresponds to the nominal regime, the 2nd term corresponds to the deviation of the nozzle throat area from the nominal regime due to the fault, and the 3rd term corresponds to the area of the hole in the rocket case. Similarly, we define the effective burning area $A_{bef}(t) = A_b(t) + \Delta A_b(t)$ as a sum of the burning area in the nominal regime and a term that describes the deviation of the burning area from the nominal regime due to the fault. Using Eqs (33) the following iterative algorithm **A1** can be introduced:

1. Set initial values of the corrections to the nozzle and burning area to zero $\Delta A_t(t) = 0$ and $\Delta A_b(t)=0$. Set values of the areas of the holes in the metal and in the insulator to constant initial values $A_m(t) = \pi \cdot R_{m0}^2$ and $A_h(t) = \pi \cdot R_{h0}^2$.
2. Update time-trace of the pressure using 1st eq. in (33)
3. Update burn web distance R, radius of the hole in the insulator R_h, and nozzle throat radius R_t using last three Eqs. In (33).
4. Repeat from the step (2) until convergence is reached.

The results of the application of this self-consistent algorithm to the prognostics of the case breach fault parameters are shown in Fig. 10(left). Once quasi-steady pressure and the dynamics of the hole growth in the insulator are predicted in the off-nominal regime one can determine the dynamics of the hole growth in the metal case and the dynamics of the fault-induced side thrust. To do so, we use the following self-consistent iterative algorithm **A2** for $t>t_0$ that takes into account the assumption that the velocity of the melting front is larger than the velocity of ablation in the insulator.

1. Set 0th approximation $R^{(0)}_{h0}(t)$ for the hole radius in the metal to r_{h0}.
2. Construct 1st approximation

$$R_m^{(1)}(t) = \begin{cases} R_m^{(0)}(t), & \text{if } R_m^{(0)}(t) > R_h(t) \\ R_h(t), & \text{if } R_m^{(0)}(t) \le R_h(t) \end{cases}$$

3. Solve Mach equation (use a maximum root)

$$M_0(t) = \begin{cases} M_0\left(1 - \dfrac{\gamma - 1}{2}M_0^2\right)^{\frac{1}{\gamma - 1}} = \dfrac{A_h}{\Gamma A_m}, & \text{if } R_m^{(0)}(t) > R_h(t) \\ \dfrac{c_t}{c_0} = \sqrt{\dfrac{2}{\gamma + 1}}, & \text{if } R_m^{(0)}(t) \le R_h(t) \end{cases}$$